Journal of Hazardous Materials 364 (2019) 300–308

Contents lists available at ScienceDirect

Journal of Hazardous Materials

journal homepage: www.elsevier.com/locate/jhazmat

Effects of resuspension on the mobility and chemical speciation of zinc in contaminated sediments

Minwei Xie[a,b,*], Marco A. Alsina[a,c], Jeffrey Yuen[a,1], Aaron I. Packman[a], Jean-François Gaillard[a,*]

[a] Department of Civil and Environmental Engineering, Northwestern University, 2145 Sheridan Road, Evanston, IL, 60208-3109, USA
[b] Marine Environmental Laboratory, Shenzhen Research Institute, The Hong Kong University of Science and Technology, Shenzhen, 518000, China
[c] Department of Construction Engineering and Management, Faculty of Engineering, University of Talca, Curicó, Chile

GRAPHICAL ABSTRACT

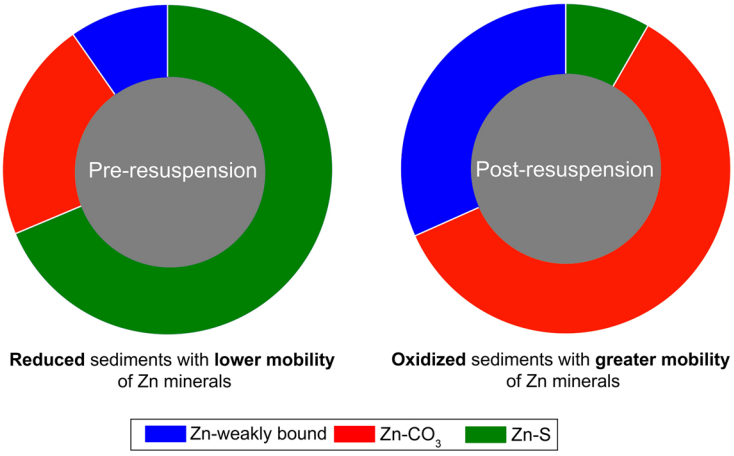

ARTICLE INFO

Keywords:
Resuspension
Contaminated sediment
Zinc mobility
Oxidative dissolution
Scavenge

ABSTRACT

Identifying and quantifying the processes governing the mobilization of metals during resuspension events is key to assessing long-term metals efflux from sediments and associated ecological impacts. We investigated the effects of sediment resuspension on the mobilization and chemical speciation of zinc in two-week-long batch experiments using metal-contaminated sediments from Lake DePue (IL, USA). Measurements of dissolved zinc and sulfate allowed us to characterize the kinetics of metal sulfide dissolution and the resulting net release of zinc to the aqueous phase. X-ray absorption spectroscopy (XAS) provided direct insights into the chemical speciation of iron and zinc and their dynamic transformations during resuspension. While ZnS rapidly oxidized during resuspension, dissolved zinc increased only after two days of resuspension. We proposed a kinetic model to explain changes in the chemical speciation of zinc during these experiments as constrained by the dissolved species concentrations and chemical speciation as informed by XAS. Only 15% of the zinc mobilized was released to the aqueous phase while the remaining fraction repartitioned the solid phase either as a carbonate precipitate or as a sorbed species. Our results show that zinc sorption onto particle surfaces and reprecipitation of zinc minerals limit zinc solubility during resuspension of metal-sulfide sediments.

* Corresponding authors at: Department of Civil and Environmental Engineering, Northwestern University, 2145 Sheridan Road, Evanston, IL, 60208-3109, USA.
E-mail addresses: minwei.xie@gmail.com (M. Xie), jf-gaillard@northwestern.edu (J.-F. Gaillard).
[1] Present address: Arcadis U.S., Inc., 200 South Michigan Ave, Suite 2000, Chicago, IL, 60604, USA.

https://doi.org/10.1016/j.jhazmat.2018.10.043
Received 2 July 2018; Received in revised form 29 September 2018; Accepted 15 October 2018
Available online 16 October 2018
0304-3894/

1. Introduction

Sediments serve as a long-term reservoir for metal contaminants and a potential contamination source to the water column. In anoxic sediments, sulfides provide a strong binding phase for divalent metals, lowering the mobility and bioavailability of metals to the surrounding benthos [1,2]. Resuspension of sediments, either by natural processes (e.g. storms, biological perturbations) or anthropogenic activities (e.g. sediment dredging), exposes anoxic sediments into oxic waters, and causes oxidative release of metals to the water column [3–5]. While dissolved metals are often cited as the most bioavailable fraction which exert negative impacts to aquatic benthos, ingestion of sediment particles also represent an important pathway for metal accumulation [6–9].

Zinc is an essential micronutrient to life but is potentially toxic at high concentrations [10]. In anoxic bedded sediments, zinc sulfide (ZnS) is the dominant phase that immobilizes zinc and limits its bioavailability [11–17]. Oxidation of ZnS is kinetically a slow process, with a reported half-life of > 30 days in oxic waters [18–21]. The persistence of ZnS could be further enhanced when clustered [19]. Therefore, presence of ZnS species in oxic water column is frequently reported [22,23]. Release of dissolved zinc during sediment resuspension is also controlled by the competition between two major processes: sulfide oxidation – which mobilizes zinc from the solid phase – and re-sequestration of released zinc in the water column by precipitation and/or adsorption reactions [24]. While numerous studies have described net metal release as an outcome of sediment resuspension, the detailed pathways are not well known [3,25,26]. In particular, kinetics of the release, the repartitioning of zinc between the solid and aqueous phase, and the effects of sediment and water composition remain poorly characterized.

Accordingly, the primary objective of this research is to improve our understanding of the mechanisms that control the mobility of zinc during sediment resuspension. The central hypothesis which we want to test is that, although the oxidative dissolution of ZnS is known to be slow when dealing with a pure mineral phase, in sediments where iron is present this reaction will be promoted. However, Zn^{2+} release to solution may be hindered by re-precipitation reactions, complexation by the organic fractions and/or surface complexation reactions. Consequently, we evaluated both the temporal evolution of bulk water chemistry and zinc speciation in the resuspended sediments. We then developed a geochemical model to simulate zinc release during resuspension by inferring particle oxidation rates and changes in Zinc speciation.

2. Materials and methods

2.1. Sediment and water collection

Sediment samples were collected from Lake DePue (LDP) (41°19′8.04″N, 89°18′39.35″W) (Fig. S1, Supporting information), a shallow backwater lake of the Illinois River historically contaminated by industrial smelting of zinc rich ores [27–29]. Our previous work showed that LDP sediments are composed primarily of fine particles, and are substantially contaminated by zinc, which is 42 times higher than the sediment quality guideline values (SQGV for zinc is 3.08 μmol/g dry sediment) [17,27–32]. At the site (Fig. S1), 20 L of overlying water was collected by hand-dipping a clean polycarbonate container (Nalgene™) beneath water surface. Meanwhile, surface sediments (~10 cm in depth) below the water was collected from a single site with a shovel to fill a 20 L plastic bucket. Sediments in sealed bucket were transported back to the laboratory immediately and stored at 4 °C, while the water was filtered through a 0.45 μm membrane filter (Millipore, USA) and then stored at the same temperature.

2.2. Sediment and water characterization

LDP sediments were characterized for particle size distribution, total recoverable metals, total organic and inorganic carbon, acid volatile sulfide (AVS) and simultaneously extracted metals (SEM) using methods reported in our previous work [30]. Dried LDP sediments were ground using an agate mortar and pestle, and loaded into a glass sample holder for x-ray diffraction (XRD) measurement. The sample holder was then mounted on a Rigaku x-ray diffractometer and scanned by varying the diffraction angle from 5° to 80° (2θ) with a step of 0.05° (2θ). The crystalline mineral composition was identified by comparing the x-ray diffractograms with the International Centre for Diffraction Data powder diffraction file database using the Jade 9 software (Materials Data Inc.)

Filtered LDP water was characterized for pH, alkalinity, dissolved organic carbon (DOC), major cation concentrations (Na^+, K^+, Ca^{2+}, Mg^{2+}, Zn^{2+}) and anion concentrations (Cl^-, NO_3^-, SO_4^{2-}, and soluble reactive phosphorus—SRP). pH was measured using a pH meter (420Aplus, Thermo Orion) and an Orion Ross combination semi-micro pH electrode calibrated with NIST-pH buffer solutions (VWR International). Alkalinity was determined by computerized titration of 50 mL of LDP water samples with 0.1 M HCl (Sigma Aldrich) using an ME-10 MTS unit from McIntosh Analytical Systems (San Jose, CA). DOC was measured with a Dohrmann Apollo 9000 High Temperature Catalytic Combustion Carbon Analyzer following EPA method 415.1. Concentrations of major cations (Na^+, K^+, Ca^{2+}, Mg^{2+}, Zn^{2+}) were determined either by Flame Atomic Emission Spectroscopy (GBC 932 A A, for Na and K) or Flame Atomic Absorption Spectroscopy (AAnalyst 100 Spectrometer, Perkin Elmer for Ca, Mg, and Zn). Concentrations of major anions (Cl^-, NO_3^-, SO_4^{2-}) were determined using a capillary ion analyzer (Waters, CIA). SRP concentration in the water, which is primarily present as phosphate species, was determined colorimetrically following EPA method 365.3.

2.3. Batch sediment resuspension experiments

Batch resuspension experiments were conducted at room temperature (21 ± 1 °C) by continuously shaking bottles containing LDP sediments and LDP water. All plastic- and glass-wares used in the experiments were cleaned by soaking them in 10% HNO_3 (v/v) for 24 h followed by rinsing three times with Milli-Q water. Sediment cores were taken from the 20 L sediment bucket and extruded (minus the top 3 cm) into a clean plastic beaker in an anaerobic chamber (3% H_2 and 97% N_2) (Coy laboratory products Inc., USA), where they were thoroughly homogenized and weighed. A mass of 2.5 g of wet homogenized sediments were weighed and added into each 250 mL HDPE bottle (25 bottles) inside an anaerobic chamber. Bottles were transferred outside of the anaerobic chamber, and 100 mL of LDP water was then added into each bottle. Twenty-five HDPE bottles containing the sediment slurries were capped and shaken at 275 rpm. To avoid CO_2 stripping, which disturbs the equilibrium of dissolved carbonate species, oxygen was provided by leaving a free headspace of ~150 cm^3 in each bottle. Sampling was conducted at 18 time intervals ranging between t = 1 and 326 h (Table S1, Supporting information). At each designated time, one or two HDPE bottles were sacrificed for water and sediment sampling. Temporal changes in water quality and sediment composition were characterized at least daily for the first 6 days (145.5 h), and an additional measurement was also performed on day 14 (326 h) to characterize the final chemical compositions of water and sediments. A total of 18 of the 25 bottles were used for analysis of water quality (dissolved oxygen (DO) concentration, dissolved metals, sulfate concentration) and sediment composition (iron and zinc speciation, total iron and zinc concentration). The remaining 7 bottles were used for AVS and SEM measurements (Table S1).

DO was directly measured in each bottle with a probe (HQ10, Hach). About 20 mL of the sediment slurry was filtered through a

0.2 µm filter (nylon, VWR International), and the filtrate was separated into two aliquots. One aliquot (10 mL) was acidified with concentrated, trace-grade HNO_3 (Sigma Aldrich) to pH < 2 and stored for dissolved metal measurements using inductively coupled plasma atomic emission spectrometry (ICP-AES, Vista-MPX, Varian). The other aliquot was used for measuring pH and stored for the determination of dissolved sulfate concentration. The sediment slurry was centrifuged under N_2 at 3414 × g for 10 min, after which the sediments were retrieved, transferred to the anaerobic chamber, and prepared for metal concentrations and speciation analysis. Thin layers of sediment samples for zinc andiron speciation analysis by XAS were collected on filter paper (0.2 µm polycarbonate, Millipore), sandwiched between two layers of Kapton tape (DuPont), stored in N_2 filled glass bottles and frozen at −80 °C until XAS analysis. Sediments were also dried at 70 °C for 48 h and stored for analysis of total metal concentrations while additional wet fractions were stored under N_2 atmosphere at −20 °C until AVS and SEM analysis. AVS was extracted by 1 M cold HCl acid, captured using 0.5 M NaOH solution and measured by colorimetry [33]. The simultaneously extracted metals were measured using ICP-AES.

2.4. X-ray absorption spectroscopy

Zinc and iron K-edge XAS spectra were measured at the DuPont-Northwestern-Dow Collaborative Access Team (DND-CAT) beamline, Sector 5 of the Advanced Photon Source, Argonne National Lab. Zinc K-edge XAS spectra were collected with an x-ray energy ranging from -100 to +600 eV above the zinc K-edge (9658 eV). Iron K-edge spectra were collected with an x-ray energy ranging from -150 to + 550 eV above the iron K-edge (7112 eV). Sediment sample spectra were collected in fluorescence mode using either a silicon drift detector (Vortex-ME4) or a 13-element HP-Ge solid state detector (Canberra). At least two scans were collected for each sample to improve the signal-to-noise ratio. Spectra for reference zinc compounds were collected in transmission mode using Oxford ionization chambers to record the incident and transmitted beam intensity. Normalized x-ray absorption near edge structure (XANES) spectra for reference iron compounds were obtained from a web-based database [34].

Data processing and analysis of sample XAS spectra were performed using the Athena software [35]. Extended x-ray absorption fine structure (EXAFS) (3–10 $Å^{-1}$) data were used to determine zinc speciation in sediments. Zinc K-edge EXAFS spectra were extracted from the normalized x-ray absorption spectra using a smooth background function ($\mu(E_0)$) calculated with the AUTOBK algorithm [30]. Since natural anoxic sediments often involve mixtures of iron species with different valences (Fe^{2+}, Fe^{3+}), iron K-edge XANES (-20 to 30 eV above absorption edge) spectra were used to determine iron speciation in sediments, as the near-edge absorption features are sensitive to the valence of iron in minerals [36]. Quantitative analysis was performed on the first derivative of iron K-edge XANES (dµ/dE) because the spectroscopic structure for the derivative XANES spectra is clearer than the absorption spectrum, and its shape is not affected by post-edge normalization procedures [37].

Zinc and iron speciation in sediment samples was determined by linear combination fitting (LCF) of sample EXAFS and XANES spectra with selected reference spectra [30,38,39]. The selection of reference spectra for LCF was achieved by performing a principal component analysis (PCA) on the ensemble of sample spectra, and a target transformation analysis (TT) on the library of reference spectra. The figure of merit used to assess the performance of LCF is the R value, which is also known as the normalized sum-squared residual values. Detailed information regarding to PCA, TT and LCF analyses are available in the supporting information.

2.5. Geochemical modeling

The results from the sediment resuspension experiments were interpreted with a kinetic geochemical model developed using PHREEQC [40]. This model integrates oxidation of metal sulfide species in suspended sediments and immobilization of zinc via precipitation of carbonates and adsorption onto HFO. Equilibrium constants for the aqueous, gas, mineral and surface complexation species were taken from the *PHREEQC* database [40]. Precipitation of zinc carbonate phases was assessed in terms of the saturation index ($SI = \log(IAP/K_{sp})$ with IAP = Ion Activity Product, and K_{sp} = solubility product), which enforced equilibration under oversaturated conditions. Equilibrium constants of zinc carbonates were obtained from the literature [41]. The geochemical model was fit to the experimental data with a Levenberg-Marquardt non-linear least squares algorithm to obtain kinetic parameters describing the oxidation of ZnS and the partitioning of Zn between the solution and the suspended sediment particles. For this purpose, two processes corresponding to two particulate fractions were considered: 1) the adsorption of zinc onto HFO, and 2) the scavenging of zinc by particulate natural organic matter (NOM), as detailed in the supporting information. The non-linear fitting procedure was implemented via the Numpy and Scipy libraries of the Python programming environment [42,43]. Further details on the kinetic model are presented in the Supporting Information.

3. Result and discussion

3.1. Initial water and sediment properties

Physicochemical characteristics of LDP sediments and water are reported in Table 1. Sediments are primarily constituted of fine particles. Zinc was identified as the primary metal contaminant, with total zinc concentration on the order of 1% by dry mass. Since SEM-Zn concentrations were greater than AVS, it strongly supports that most, if not all, of the sulfides were present as ZnS [44]. The sediment contained a significant amount of inorganic carbon (2.66% by mass), predominantly under the form of calcium and zinc carbonates [27]. XRD results evidenced the presence of crystalline inorganic carbonate minerals, mainly calcite and dolomite (Fig. 1). LDP water was slightly basic (pH 7.8) with high alkalinity (5.8 meq L^{-1}). LDP water also contained a significant concentration of sulfate (1.9 mM), which is characteristic of water bodies affected by mining and smelting activities [45–47].

3.2. Water quality during sediment resuspension

The effects of sediment resuspension on DO, pH, dissolved zinc and

Table 1
Physico-chemical Properties of LDP Sediment and Water.

LDP Sediment		LDP Water	
Grain size		pH	7.8
< 45 µm (%)	81	Alkalinity (meq/L)	5.84 (± 0.02)
45-106 µm (%)	6	Ca^{2+} (mM)	3.17 (± 0.08)
> 106 µm (%)	13	Mg^{2+} (mM)	0.77 (± 0.09)
Organic carbon (% w/w)	3.09	Na^{+} (mM)	3.01 (± 0.09)
Inorganic carbon (% w/w)	2.66	K^{+} (mM)	0.15 (± 0.01)
AVS (µmol/g dry sediment)	91.6 (± 4.4)	Zn^{2+} (µM)	0.92 (± 0.06)
SEM-Zn (µmol/g dry sediment)	116 (± 6)	SRP (mM)	0.022 (± 0.001)
Total Zn (µmol/g dry sediment)	131 (± 17)	DOC (mg C/L)	9.1 (± 0.4)
Total Cu (µmol/g dry sediment)	6.91 (± 0.43)	Cl^{-} (mM)	2.7 (± 0.3)
Total Fe (µmol/g dry sediment)	610 (± 30)	NO_3^{-} (mM)	0.25 (± 0.02)
		SO_4^{2-} (mM)	1.9 (± 0.2)

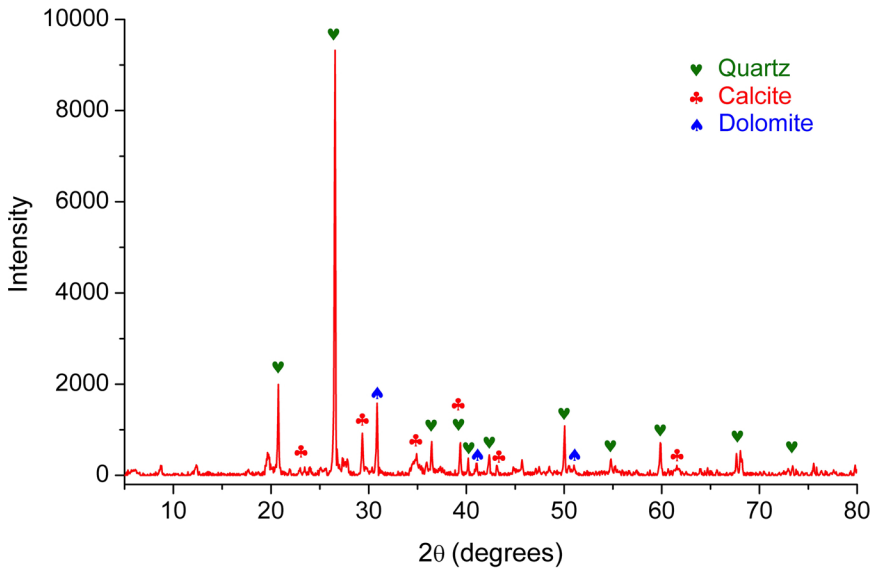

Fig. 1. X-ray diffraction pattern of Lake DePue sediments, with spectral features of mineral phases indicated.

sulfate concentration are shown in Figs. 2 and S2. DO maintained a concentration of 238 ± 5 μM during the first 75 h, and gradually declined to 151 μM over the remainder of the experiment (Fig. S2a). pH of the water evolved from slightly basic (7.9) to neutral (7.0) over the course of the experiment (Fig. S2b). Dissolved zinc increased slowly during the first 48 h of resuspension, and then rapidly increased to a final concentration of 170 μM Zn^{2+} (Fig. 2a). The difference in dissolved Zn^{2+} concentration between the onset and the end of the experiment indicated a total release of 0.169 μmoles of zinc from the 2.5 g of resuspended sediment. Dissolved sulfate increased at a rate of 7.59 μM/h for the first 146 h. For the remainder of the experiment (~179 h), dissolved sulfate concentration only marginally increased. The difference between the initial and final sulfate concentration indicated a net release of 116 μmoles of sulfate during the resuspension experiment.

3.3. Fe speciation during sediment resuspension

First derivatives of iron K-edge XANES spectra of sediment samples are shown in Fig. 3. All sample spectra were characterized with two strong peaks and one weak peak near the absorption edge. Notably, the derivative XANES spectrum of the initial sediment sample (t = 0 h) has a weak peak located to the right of the other two strong peaks, while the derivative XANES spectra for the remaining sediment samples have a weak peak located to the left of the other two strong peaks (Fig. 3a, b). The difference in location of the weak peak suggests a change in the coordination environment of iron in the sediment immediately after the onset of sediment resuspension.

PCA analysis of the entire sediment sample dataset and TT analysis through the library of reference spectra identified two dominant iron species in LDP sediments, aegirine ($NaFe^{(III)}Si_2O_6$) and ferrihydrite (Fig. S4, Supporting information). Aegirine is an igneous mineral that typically forms under high temperature (350 to 500 °C) from hematite (Fe_2O_3) in the presence of NaCl and silica (SiO_2) [48], and has been reported as a common mineral phase in smelting slags [49]. Inclusion of an additional iron species, vivianite ($(Fe^{(II)})_3(PO_4)_2 \cdot 8H_2O$), in the LCF analysis of the initial sediment spectrum (t = 0 h), substantially improved the fit quality (R valued decreased by 24.8%). However, adding vivianite into the LCF of other remaining sediment spectra did not improve the reconstruction results, suggesting this phase underwent rapid oxidation after resuspension.

LCF analysis showed that the original LDP sediments comprised ~67% aegirine, ~18% ferrihydrite, and ~15% vivianite (Fig. 3c). The aegirine fraction remained about constant at 64.6 ± 6.2%, indicating little to no change affecting this mineral phase during resuspension. However, vivianite (14.7%) disappeared within 1 h after the onset of resuspension. Ferrihydrite increased correspondingly (15.5%) during the first hour, and thereafter remained nearly constant at 35.7 ± 6.5% for the remainder of the experiment. The rapid and concurrent removal of Fe(II) vivianite and increase in Fe(III) ferrihydrite supports the conclusion that reduced Fe(II) rapidly oxidized during resuspension, leading to the formation of HFO.

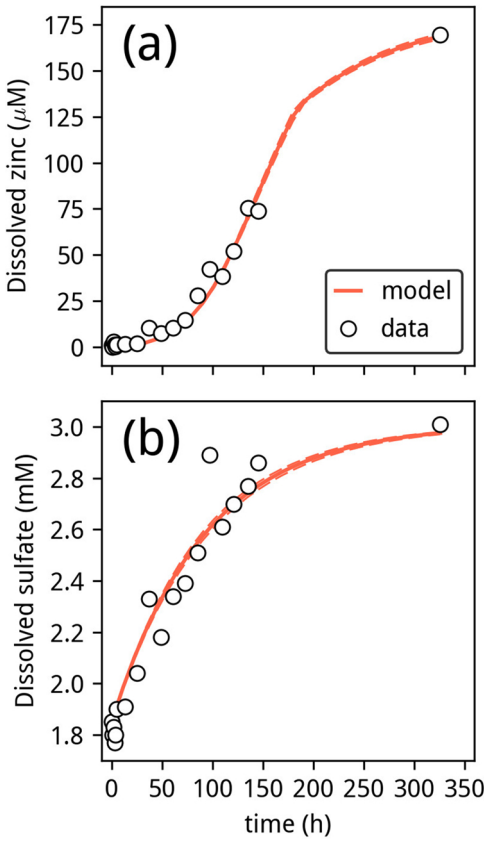

Fig. 2. Release of zinc (a) and sulfate (b) during the resuspension experiment. Solid lines represent the estimated concentrations from the geochemical model (solid lines)., including the standard errors (dashed lines).

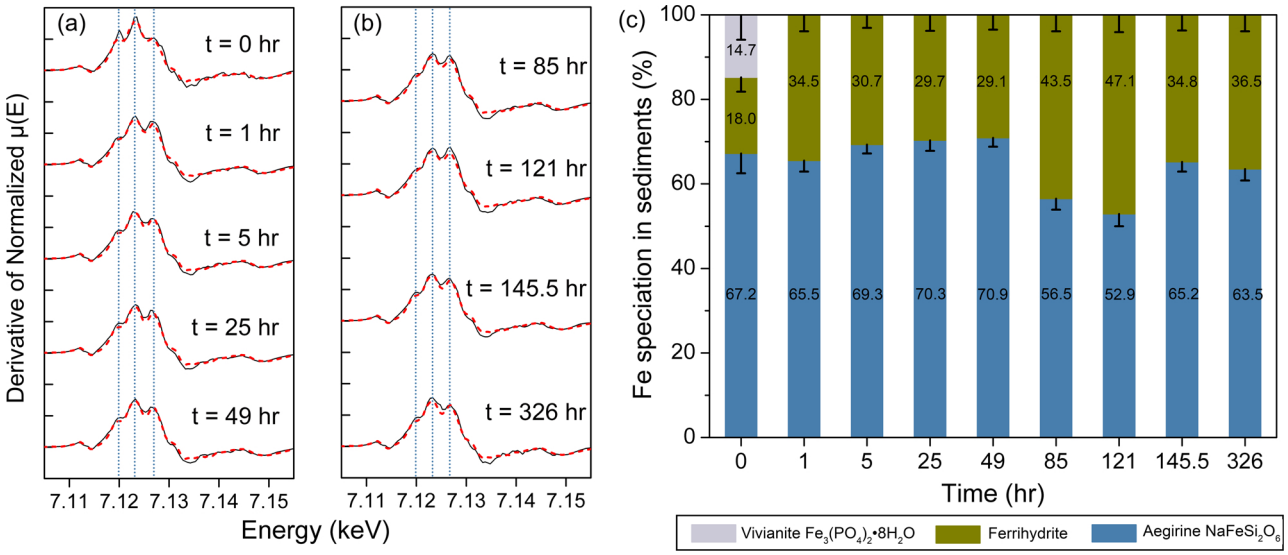

Fig. 3. (a) (b) First derivative iron K edge XANES spectra (solid black lines) and LCF reconstructed curves (dashed red lines) for all experimental samples. Three reference phases – vivianite, ferrihydrite, and aegirine – were used for the LCF reconstruction. Vertical dotted lines indicate the three peaks near the absorption edge. (c) Evolution of iron speciation during the resuspension experiment. (For interpretation of the references to colour in this figure legend, the reader is referred to the web version of this article).

3.4. Zinc speciation during sediment resuspension

Zinc K-edge EXAFS spectra of sediment samples are shown in Fig. 4a, b. At the beginning of the experiment, Zinc EXAFS spectra were characterized by four oscillations in k-space ranging from 3 to 10 Å. As resuspension time increased, the first two oscillations shifted toward lower k and the amplitude of two other oscillations diminished, indicating changes in the immediate coordination environment of zinc in LDP sediments over time.

PCA analysis of the entire sediment sample dataset and TT analysis through the library of reference spectra identified three dominant zinc species in LDP sediments: ZnS, $Zn_5(CO_3)_2(OH)_6$ (referred to as $Zn-CO_3$ hereafter), and Zn^{2+} sorbed onto ferrihydrite (referred to as Zn-HFO) (Fig. S3, Supporting information). Our previous XAS studies of LDP sediments also identified zinc hexa-coordinated with water oxygen as a dominant species in oxidized sediments (hereafter referred to as Zn-aq). This phase encompasses both true aqueous zinc species and weak outer-sphere zinc surface complexes [16,17,30,31]. LCF with the four reference species successfully reproduced all features of the EXAFS spectra (Fig. 4a, b, Table S3). Concentrations of each zinc species were calculated by multiplying the fraction of each zinc species identified by LCF (Fig. 4c) with the measured total zinc concentration in each sediment sample (Fig. S5).

LCF analysis indicated that bulk LDP sediment comprised ~70% of Zn-S, ~20% of $Zn-CO_3$, and ~10% of Zn-aq fractions (Fig. 4c). After onset of resuspension, the Zn-S fraction decreased gradually with time, reaching 11.1% at t = 121 h, and then remained approximately constant from t =121 to 326 h. Zn-HFO was not detected initially, but emerged after 1 h of resuspension. The Zn-HFO fraction increased gradually from 6.9% at t = 1 h to 32.8% at t = 49 h, then varied between t = 49 h and t = 145.5 h, and eventually disappeared by t = 326 h. The $Zn-CO_3$ fraction was constant at 28.0 ± 4.0% from t = 1 h

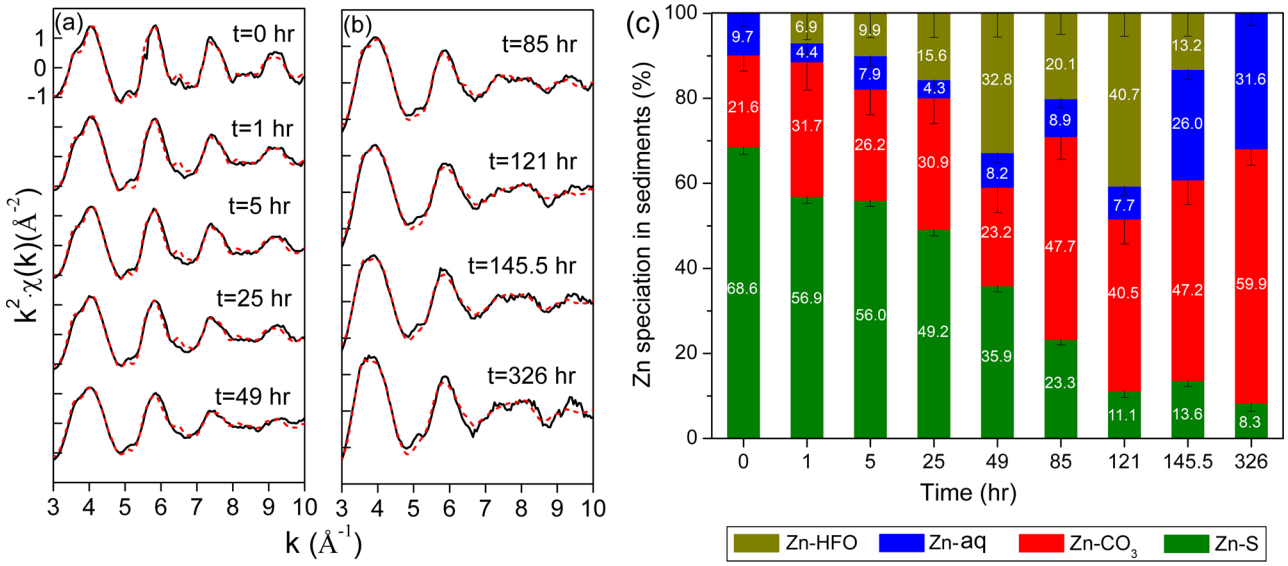

Fig. 4. (a)(b) EXAFS spectra (solid black lines) and LCF reconstructed curves (dashed red lines) for all experimental samples. Four reference species – Zn-HFO, Zn-aq, $Zn-CO_3$, and Zn-S – were used for the LCF reconstruction. (c) Evolution of zinc speciation during the resuspension experiment. (For interpretation of the references to colour in this figure legend, the reader is referred to the web version of this article).

to t = 49 h, and then significantly increased to 47.7 ± 8.1% between t = 85 h and t = 326 h ($p < 0.05$, one-way ANOVA). The Zn-aq fraction was nearly constant at 6.9 ± 2.0% for the first 121 h and then increased to ~26% at t =145.5 h and ~32% at t = 326 h.

Corresponding concentrations of each zinc species are shown in Fig. S5. Zn-S concentration in the suspended sediments gradually decreased from 99.0 μmoles/g at t = 0 h to 9.1 μmoles/g at t = 326 h. Considering the mass of sediments introduced (1.27 g dry sediment), this represented a loss of 114 μmoles Zn-S from the sediment. Zn-HFO concentrations in suspended sediments gradually increased from 8.3 μmoles/g at t = 1 h to 44.1 μmoles/g at t = 49 h. Zn-HFO concentrations then varied for the next 96.5 h and eventually disappeared. Zn−CO3 concentrations were nearly constant at 35.9 ± 5.2 μmoles/g for the first 49 h, and then significantly increased to 60.9 ± 4.9 μmoles/g between t = 85 h and t = 326 h ($p < 0.01$, one-way ANOVA). Zn-aq concentrations were constant at 9.0 ± 2.8 μmoles/g for the first 121 h and then increased to 35.3 μmol/g at t = 326 h.

3.5. Geochemical modeling

The resuspension experiment showed a net release of 116 μmoles of sulfate to the water column, similar to the amount of Zn-S being oxidized (114 μmoles). Therefore, we assume that the main process that governs the release of sulfate and zinc is the oxidation of ZnS from the mineral assemblage:

$$ZnS_{(s)} + 2O_2 \leftrightarrow Zn^{2+} + SO_4^{2-} \quad (1)$$

Because dissolved sulfate concentration is not influence by solution pH and the presence of reactive surfaces, the kinetics of ZnS oxidation was estimated in terms of the release rate of dissolved sulfate during resuspension [50]. The release rate of sulfate remained linear during the first 150 h of the experiment, but decreased considerably thereafter (Fig. 2b). This rate decrease was likely caused by the depletion of readily-oxidizable ZnS in the resuspended sediment, which limited the production of sulfate. Correspondingly, a pseudo first-order kinetic expression was used to model the oxidation of ZnS and the release of dissolved sulfate:

$$\frac{d[ZnS]}{dt} = -K_r \cdot [ZnS] \quad (2)$$

where K_r is the reaction rate for the oxidation of ZnS (hr^{-1}), and [ZnS] is the amount of ZnS (mol) being oxidized. The analytical solution of Eq. (2) is:

$$[ZnS] = [ZnS]_0 \cdot e^{-K_r \cdot t} \quad (3)$$

where $[ZnS]_0$ is the initial amount of ZnS available for oxidation, which was estimated in 116 μmoles based on the observed release of sulfate during the experiment. The parameter K_r was found to be 3.01 ± 0.12 × 10^{-7} hr^{-1} via a nonlinear least-squares fit of the measured dissolved sulfate concentration during the resuspension experiment.

While Eq. (1) indicates that dissolution of ZnS should release equivalent amounts of Zn^{2+} and sulfate, the observed release of dissolved sulfate (116 μmoles) was much greater than the release of dissolved Zn^{2+} (17 μmoles) (Fig. 2). This difference indicates that most of the Zn^{2+} (~85.3%) mobilized by ZnS dissolution was retained or resequestered in the solid phase. Since adsorption and precipitation are the two primary processes that control the solubility of metals in oxic environments [51–55], they were both considered in the geochemical model. Adsorption was modeled using a surface-complexation approach [56]. However, the application of surface complexation models to sediments is delicate because of the complexity of the mineral assemblages present [57]. In many instances, studies investigating metal sorption in sediments commonly refer to iron-oxide coatings onto particle surfaces as the primary controlling factor [58]. Simulation of Zn^{2+} adsorption onto HFO in these resuspended sediments is justified by a set of independent observations (Figs. 3,4):

i) There is a significant ferrihydrite fraction in the resuspended sediments;
ii) Oxidative dissolution of vivianite during resuspension is likely to form fresh ferrihydrite precipitates;
iii) XAS analysis confirmed zinc sorption onto ferrihydrite in the resuspended sediments.

Following the later observations, the concentration of HFO in the model was estimated to be ~610 μmol/g, as the measured concentration of iron in the sediments was 610 ± 27 μmol/g. Precipitation processes were incorporated into the model by performing thermodynamic equilibrium calculations at each time step to determine the saturation indices of ferrihydrite and hydrozincite ($Zn_5(CO_3)_2(OH)_6$), and then enforcing solution equilibrium with these solid phases if the IAP was greater than the solubility product.

Modeling results of Zn^{2+} and sulfate are shown in Fig. 2. The kinetic model successfully reproduced the observed changes in dissolved sulfate and Zn^{2+} concentration with time under oxic conditions. The simulated sulfate concentration increased exponentially to an upper limit, suggesting depletion in readily available particle associated metal-sulfide.

The simulation also successfully reproduced the observed trends in solid zinc species in the sediments (Fig. 5). The simulated fraction of Zn-S decreased exponentially during resuspension, in agreement with the XAS speciation results. These simulations also indicate that hydrozincite remained undersaturated during the first 191 h of the resuspension experiment (SI < 0), but saturated during the remainder of the experiment. Consequently, the evolution in Zn-CO_3 fraction observed in the XAS signal of the mineral assemblage throughout the resuspension experiment cannot be solely interpreted in terms of thermodynamic equilibrium reactions with hydrozincite. The presence of a zinc-carbonate fraction, as documented by XAS, while the solution remains undersaturated with respect to hydrozincite suggests that zinc is either co-entrained/substituted into the carbonate fraction [59] or that it is sorbed to the surface of carbonate minerals [60]. On the other hand, the simulated Zn-HFO fraction, including both strong and weak zinc surface complexes, as well as zinc scavenged by NOM, matched well the sum of the measured Zn-HFO and Zn-aq fractions. By the end of the resuspension experiment (t = 326 h), the simulation predicts a mineral assemblage containing 45% hydrozincite, 38% zinc bound to HFO, 15% zinc bound to NOM, and 2% remaining as ZnS.

3.6. Processes controlling mobility of zinc during resuspension

In anoxic sediments, metal sulfides are often the predominant solid phases that immobilize metals [61]. At equilibrium, the formation of metal sulfides follows the “sulfide ladder”, where precipitation of more insoluble metal sulfides prevails over the formation of less insoluble metal sulfides [23,62]. The solubility product of ZnS is 5 orders of magnitude lower than that of FeS [63,64]. Therefore, at equilibrium and in excess of zinc compared to sulfide, ZnS is expected to be the dominant metal sulfide species in LDP sediments. ZnS is also expected to control zinc sequestration in LDP as both SEM-Zn and total zinc concentrations were in great excess of AVS (Table 1). Speciation results for iron and zinc also support these predictions: Zn-S accounted for ~69% of the zinc in LDP sediments (Fig. 4c) and the Zn-S concentration (99 μmol/g) was similar to the measured AVS concentration (91.6 μmol/g) (Fig. S6, Supporting Information). Further, Fe(II) occurred as vivianite ($(Fe^{(II)})_3(PO_4)_2 \cdot 8H_2O$) in LDP sediments, and FeS was not present (Fig. 3c, Fig. S4, Supporting information).

Anoxic sediments are oxidized in presence of dissolved O_2 during resuspension events, which can potentially release metals to the water column. ZnS is normally considered to be very resistant to oxidation by dissolved O_2. However, our results showed that ZnS oxidation occurred

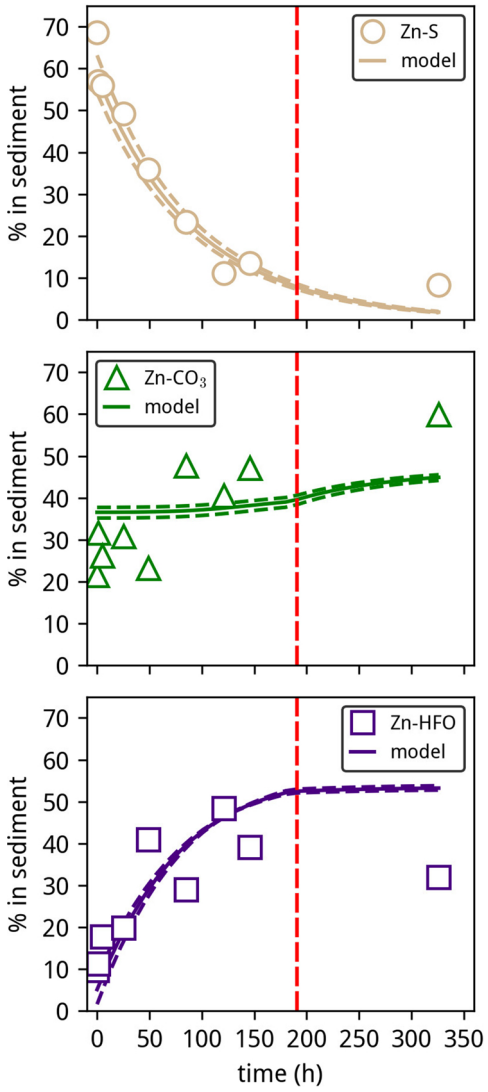

Fig. 5. Evolution of zinc speciation in the sediments during the resuspension experiment. Scattered points represent the zinc speciation determined by LCF analysis of the zinc K-edge EXAFS spectra (from Fig. 4), while solid lines represent the speciation results from the geochemical model, including the standard errors (dashed lines). The red vertical dashed line indicates the time after which the solution was saturated with respect to hydrozincite. (For interpretation of the references to colour in this figure legend, the reader is referred to the web version of this article).

at a much faster rate under our experimental conditions, with ~85% of sediment ZnS oxidized within 120 h of resuspension. ZnS oxidation is generally regarded as a complex process involving several intermediate steps, with some catalyzed by microbial species enzymes while others are purely chemical [65–67]. In oxic waters, oxidation of ZnS is driven either by abiotic reduction of Fe^{3+} to Fe^{2+} or directly by dissolved O_2 [68–71]:

$$ZnS_{(s)} + 2Fe^{3+} \leftrightarrow Zn^{2+} + S^0 + 2Fe^{2+} \quad (4)$$

$$ZnS_{(s)} + 0.5\,O_2 + 2H^+ \leftrightarrow Zn^{2+} + S^0 + H_2O \quad (5)$$

Fe^{2+} is rapidly oxidized by dissolved oxygen under circum-neutral pH condition [72,73], while oxidation of elemental sulfur (S°) to sulfate (SO_4^{2-}) has been shown to be microbially mediated, particularly by bacteria such as *Thiobacillus thiooxidans* and *Thiobacillus ferrooxidans* [69,70,74–77]. In this case, the resulting reactions are thought to be:

$$2Fe^{2+} + \frac{1}{2}O_2 + 2H^+ \leftrightarrow 2Fe^{3+} + H_2O \quad (6)$$

$$Fe^{3+} + 3H_2O \leftrightarrow Fe(OH)_{3(s)} + 3H^+ \quad (7)$$

$$S^0 + \frac{3}{2}O_2 + H_2O \leftrightarrow SO_4^{2-} + 2H^+ \quad (8)$$

Therefore, the combination of the cyclic Fe^{3+}/Fe^{2+} redox couple and the bio-oxidation of elemental sulfur are the likely processes leading to the oxidative dissolution of ZnS observed during these resuspension experiments [69,78]. Assuming that the Fe^{3+}/Fe^{2+} redox cycle is not a limiting factor, which is likely the case given iron concentrations present in LDP sediments, these intermediate reaction steps lead to the global oxidation of ZnS that mobilizes Zn^{2+} and SO_4^{2-} in a 1:1 M ratio, as described overall by Eq. (1).

The preceding analysis applies for primary dissolution of ZnS from resuspended sediments, but direct measurements of solution chemistry indicate that additional processes rapidly scavenged much of the released zinc. The overall released SO_4^{2-} (116 µmoles) was 7 times greater than the released zinc (17 µmoles), indicating that most (~85%) of the zinc released from ZnS oxidation was retained or resequestered in the solid phase. Zinc K-edge EXAFS speciation analysis and geochemical modeling revealed that adsorption onto HFO and hydrozincite/carbonate precipitation are the two major processes that re-incorporate zinc into resuspended particles (Figs. 4c, 5). These two processes led to increasing fractions of zinc carbonate and/or weak Zn^{2+} surface complexes in the resuspended sediments. Since the solubility of these two fractions are strongly pH dependent, the degree of metal release during sediment resuspension is mediated by the acidity produced during oxidation and the buffering capacity of the aqueous and sediment phases [52].

As the overall oxidative dissolution of ZnS does not produce acidity (Eq. (1)), the oxidation of Fe(II) to form HFO/$Fe(OH)_3$ is generally considered to be an important process that releases protons (Eqs. (5), (6)) [79–82]. However, we found that solution pH only dropped modestly (from 7.8 to 7.0) during resuspension. Several buffering mechanisms may act in concert to neutralize the produced acidity: i) Phosphate released by dissolution of vivianite during resuspension; ii) High alkalinity of LDP water; iii) Presence of carbonate minerals such as calcite and dolomite in LDP sediments (Fig. 1).

3.7. Implications of resuspension-induced changes for metals bioavailability

The present study provides direct insights into the release and partitioning behavior of sediment-bound zinc during a resuspension event. While oxidative dissolution of ZnS as a pure mineral phase has frequently been cited as a slow process, we observed promoted dissolution rates for this phase in the present experiment. It is likely that other processes occurring when the mixed assemblage of sediments were resuspended facilitated the oxidation of ZnS. This suggests that behavior of metal contaminants in mixed mineral assemblages differs from that of a pure mineral. Therefore, when performing risk assessment involving sediment resuspension, fully relying on the reported oxidative dissolution kinetics of pure minerals may lead to biased assessment of environmental risk.

During the resuspension, only a limited fraction of zinc (~15%) released by oxidation of primary solid-phase ZnS was mobilized to the solution as Zn^{2+}, and most of the released zinc was re-sequestered in other solid phases (HFO, carbonate/hydrozincite). The re-sequestered zinc was primarily associated in more labile forms — carbonates and surface complexes —that have substantially greater mobility and bioavailability than ZnS [83,84]. Enhanced mobilization of zinc from these solid phases would be expected if acidification were occurring during the resuspension. Resuspension of contaminated sediments in waters with weak buffering capacity (low alkalinity) may therefore represent higher risk in metal release.

Ingestion of sediment particles by aquatic benthos (deposit feeder or filter feeders) often constitutes an important route to accumulate metals from contaminated sediments. Resuspended sediments containing metals in a more bioavailable form may poses higher toxicity to the benthos and affect the ecological health of waters overlying metal contaminated sediments.

Acknowledgments

This research was supported by the Strategic Environmental Research and Development Program (ER-1745) and by the National Natural Science Foundation of China (Grant 21707113). We thank Dr. Qing Ma for his technical assistance while performing XAS experiments at the APS. Portions of this work were performed at the DND-CAT Synchrotron Research Center located at Sector 5 of the APS. DND-CAT is supported by the E.I. DuPont de Nemours & Co., The Dow Chemical Company, the U.S. National Science Foundation through Grant DMR-9304725, and the State of Illinois through the Department of Commerce and the Board of Higher Education Grant IBHE HECA NWU 96.

Appendix A. Supplementary data

Supplementary material related to this article can be found, in the online version, at doi:https://doi.org/10.1016/j.jhazmat.2018.10.043.

References

[1] T.M. Remaili, N. Yin, W.W. Bennett, S.L. Simpson, D.F. Jolley, D.T. Welsh, Contrasting effects of bioturbation on metal toxicity of contaminated sediments results in misleading interpretation of the AVS–SEM metal-sulfide paradigm, Environ. Sci.: Process. Impacts 20 (2018) 1285–1296.
[2] M. Xie, N. Wang, J.-F. Gaillard, A.I. Packman, Hydrodynamic forcing mobilizes Cu in low-permeability estuarine sediments, Environ. Sci. Technol. 50 (2016) 4615–4623.
[3] S.L. Simpson, S.C. Apte, G.E. Batley, Effect of short-term resuspension events on trace metal speciation in polluted anoxic sediments, Environ. Sci. Technol. 32 (1998) 620–625.
[4] S.L. Simpson, S.C. Apte, G.E. Batley, Effect of short-term resuspension events on the oxidation of cadmium, lead, and zinc sulfide phases in anoxic estuarine sediments, Environ. Sci. Technol. 34 (2000) 4533–4537.
[5] M. Xie, N. Wang, J.-F. Gaillard, A.I. Packman, Interplay between flow and bioturbation enhances metal efflux from low-permeability sediments, J. Hazard. Mater. 341 (2018) 304–312.
[6] S.L. Simpson, C.K. King, Exposure-pathway models explain causality in whole-sediment toxicity tests, Environ. Sci. Technol. 39 (2005) 837–843.
[7] C.E. Schlekat, A.W. Decho, G.T. Chandler, Bioavailability of particle-associated silver, cadmium, and zinc to the estuarine amphipod Leptocheirus plumulosus through dietary ingestion, Limnol. Oceanogr. 45 (2000) 11–21.
[8] R. Weltens, R. Goossens, S. Van Puymbroeck, Ecotoxicity of contaminated suspended solids for filter feeders (Daphnia magna), Arch. Environ. Contam. Toxicol. 39 (2000) 315–323.
[9] N.A. Hill, C.K. King, L.A. Perrett, E.L. Johnston, Contaminated suspended sediments toxic to an Antarctic filter feeder: aqueous-and particulate-phase effects, Environ. Toxicol. Chem.: Int. J. 28 (2009) 409–417.
[10] G.J. Fosmire, Zinc toxicity, Am. J. Clin. Nutr. 51 (1990) 225–227.
[11] W. Calmano, J. Hong, U. Forstner, Binding and mobilization of heavy metals in contaminated sediments affected by pH and redox potential, Water Sci. Technol. 28 (1993) 223–235.
[12] V.M. Shul'kin, N.N. Bogdanova, Mobilization of zinc, copper, cadmium, and lead in aerated seawater from a suspension of bottom sediments, Oceanology 38 (1998) 620–627.
[13] M.A. Huerta-Diaz, A. Tessier, R. Carignan, Geochemistry of trace metals associated with reduced sulfur in freshwater sediments, Appl. Geochem. 13 (1998) 213–233.
[14] J.W. Morse, G.W. Luther Iii, Chemical influences on trace metal-sulfide interactions in anoxic sediments, Geochim. Cosmochim. Acta 63 (1999) 3373–3378.
[15] E.F. Peltier, S.M. Webb, J.F. Gaillard, Zinc and lead sequestration in an impacted wetland system, Adv. Environ. Res. 8 (2003) 103–112.
[16] S.M. Webb, The Chemistry of Zinc-Microbe Interactions in the Sediments of Lake, Northwestern University, DePue, IL, 2001.
[17] S.M. Webb, J.-F. Gaillard, Zinc speciation in contaminated sediments: quantitative determination of zinc coordination by X-ray absorption spectroscopy, Aquat. Geochem. 21 (2015) 295–312.
[18] K. Sukola, F.Y. Wang, A. Tessier, Metal-sulfide species in oxic waters, Anal. Chim. Acta 528 (2005) 183–195.
[19] T.F. Rozan, M.E. Lassman, D.P. Ridge, G.W. Luther III, Evidence for iron, copper and zinc complexation as multinuclear sulphide clusters in oxic rivers, Nature 406 (2000) 879–882.
[20] K.C. Bowles, R.A. Bell, M.J. Ernste, J.R. Kramer, H. Manolopoulos, N. Ogden, Synthesis and characterization of metal sulfide clusters for toxicological studies, Environ. Toxicol. Chem. 21 (2002) 693–699.
[21] E. Peltier, Trace Metal Speciation and Availability in a Contaminated Freshwater Wetland Located in Chicago, Illinois, (2003).
[22] G.W. Luther, D.T. Rickard, Metal sulfide cluster complexes and their biogeochemical importance in the environment, J. Nanoparticle Res. 7 (2005) 389–407.
[23] C. Priadi, P. Le Pape, G. Morin, S. Ayrault, F. Maillot, F. Juillot, R. Hochreutener, I. Llorens, D. Testemale, O. Proux, X-ray absorption fine structure evidence for amorphous zinc sulfide as a major zinc species in suspended matter from the Seine River downstream of Paris, Ile-de-France, France, Environ. Sci. Technol. 46 (2012) 3712–3720.
[24] H.J. Shipley, Y. Gao, A.T. Kan, M.B. Tomson, Mobilization of metals and inorganic compounds during resuspension of anoxic sediment, ACS National Meeting, (2005), pp. 630–638.
[25] J. Eggleton, K.V. Thomas, A review of factors affecting the release and bioavailability of contaminants during sediment disturbance events, Environ. Int. 30 (2004) 973–980.
[26] M.R. Stanton, Baseline laboratory studies of sphalerite (ZnS) dissolution: effects on aqueous metal concentrations and solubilization rates, Proceedings 22nd National Conference (2005) 1155–1165.
[27] H.L. Gough, A.L. Dahl, M.A. Nolan, J.F. Gaillard, D.A. Stahl, Metal impacts on microbial biomass in the anoxic sediments of a contaminated lake, J. Geophys. Res.-Biogeosci. 113 (2008).
[28] H.L. Gough, A.L. Dahl, E. Tribou, P.A. Noble, J.F. Gaillard, D.A. Stahl, Elevated sulfate reduction in metal-contaminated freshwater lake sediments, J. Geophys. Res.-Biogeosci. 113 (2008).
[29] S.M. Webb, G.G. Leppard, J.-F. Gaillard, Zinc speciation in a contaminated aquatic environment: characterization of environmental particles by analytical electron microscopy, Environ. Sci. Technol. 34 (2000) 1926–1933.
[30] M. Xie, B.A. Jarrett, C. Da Silva-Cadoux, K.J. Fetters, G.A. Burton, J.-F. Gaillard, A.I. Packman, Coupled effects of hydrodynamics and biogeochemistry on Zn mobility and speciation in highly contaminated sediments, Environ. Sci. Technol. 49 (2015) 5346–5353.
[31] J.F. Gaillard, S.M. Webb, J.P.G. Quintana, Quick X-ray absorption spectroscopy for determining metal speciation in environmental samples, J. Synchrotron Radiat. 8 (2001) 928–930.
[32] S. Simpson, G. Batley, Sediment Quality Assessment: a Practical Guide, CSIRO PUBLISHING, Collingwood, Vic, Australia, 2016.
[33] H. Allen, G. Fu, W. Boothman, D. Di Toro, J. Mahony, Determination of Acid Volatile Sulfide and Selected Simultaneously Extractable Metals in Sediment, Office of Water Regulations and Standards, US Environmental Protection Agency, Washington, DC, 1991.
[34] E.J. Houwing, Determination of the critical erosion threshold of cohesive sediments on intertidal mudflats along the Dutch Wadden Sea coast, Estuar. Coast. Shelf Sci. 49 (1999) 545–555.
[35] B. Ravel, M. Newville, ATHENA, ARTEMIS, HEPHAESTUS: data analysis for X-ray absorption spectroscopy using IFEFFIT, J. Synchrotron Radiat. 12 (2005) 537–541.
[36] A. Manceau, A.I. Gorshkov, V.A. Drits, Structural chemistry of Mn, Fe, Co, and Ni in manganese hydrous oxides; Part I, information from XANES spectroscopy, Am. Mineral. 77 (1992) 1133–1143.
[37] A. Manceau, M.A. Marcus, S. Grangeon, Determination of Mn valence states in mixed-valent manganates by XANES spectroscopy, Am. Mineral. 97 (2012) 816–827.
[38] A. Van Damme, F. Degryse, E. Smolders, G. Sarret, J. Dewit, R. Swennen, A. Manceau, Zinc speciation in mining and smelter contaminated overbank sediments by EXAFS spectroscopy, Geochim. Cosmochim. Acta 74 (2010) 3707–3720.
[39] C. Da Silva-Cadoux, L. Zanella, J.-F. Gaillard, Selecting reference compounds for determining chemical speciation by X-ray absorption spectroscopy, J. Anal. At. Spectrom. 27 (2012) 957–965.
[40] D.L. Parkhurst, C. Appelo, Description of input and examples for PHREEQC version 3: a computer program for speciation, batch-reaction, one-dimensional transport, and inverse geochemical calculations, US Geological Survey, (2013).
[41] P. Schindler, M. Reinert, H. Gamsjäger, Zur Thermodynamik der Metallcarbonate 3. Mitteilung [1]. Löslichkeitskonstanten und Freie Bildungsenthalpien von ZnCO3 und Zn5 (OH) 6 (CO3) 2 bei 25°, Helv. Chim. Acta 52 (1969) 2327–2332.
[42] T.E. Oliphant, Python for scientific computing, Comput. Sci. Eng. 9 (2007) 10–20.
[43] Svd. Walt, S.C. Colbert, G. Varoquaux, The NumPy Array: A Structure for Efficient Numerical Computation, Comput. Sci. Eng. 13 (2011) 22–30.
[44] J.S. Lee, B.G. Lee, S.N. Luoma, H.J. Choi, C.H. Koh, C.L. Brown, Influence of acid volatile sulfides and metal concentrations on metal partitioning in contaminated sediments, Environ. Sci. Technol. 34 (2000) 4511–4516.
[45] M.B. Lindsay, M.C. Moncur, J.G. Bain, J.L. Jambor, C.J. Ptacek, D.W. Blowes, Geochemical and mineralogical aspects of sulfide mine tailings, Appl. Geochem. 57 (2015) 157–177.
[46] J.N. Moore, S.N. Luoma, Hazardous wastes from large-scale metal extraction. A case study, Environ. Sci. Technol. 24 (1990) 1278–1285.
[47] O. Karnachuk, A. Gerasimchuk, D. Banks, B. Frengstad, G. Stykon, Z. Tikhonova, A. Kaksonen, J. Puhakka, A. Yanenko, N. Pimenov, Bacteria of the sulfur cycle in the sediments of gold mine tailings, Kuznetsk Basin, Russia, Microbiology 78 (2009) 483–491.
[48] P.L. McSwiggen, G.B. Morey, J.M. Cleland, The origin of aegirine in iron formation of the Cuyuna Range, east-central Minnesota, Can. Mineral. 32 (1994) 589–598.
[49] V. Ettler, O. Legendre, F. Bodénan, J.-C. Touray, Primary phases and natural weathering of old lead–zinc pyrometallurgical slag from Příbram, Czech Republic, Can. Mineral. 39 (2001) 873–888.

[50] D. Rickard, J.W. Morse, Acid volatile sulfide (AVS), Mar. Chem. 97 (2005) 141–197.
[51] G.E. Brown, A.L. Foster, J.D. Ostergren, Mineral surfaces and bioavailability of heavy metals: a molecular-scale perspective, Proc. Natl. Acad. Sci. 96 (1999) 3388–3395.
[52] Y.S. Hong, K.A. Kinney, D.D. Reible, Acid volatile sulfides oxidation and metals (Mn, Zn) release upon sediment resuspension: laboratory experiment and model development, Environ. Toxicol. Chem. 30 (2011) 564–575.
[53] P.A. O'Day, S.A. Carroll, G.A. Waychunas, Rock – water interactions controlling zinc, cadmium, and lead concentrations in surface waters and sediments, U.S. tri-state mining district. 1. Molecular identification using X-ray absorption spectroscopy, Environ. Sci. Technol. 32 (1998) 943–955.
[54] P.A. O'Day, S.A. Carroll, G.A. Waychunas, B. Phillips, Proceedings of the 8th International Conference on X-ray absorption fine StructureXAS of trace element coordination in natural sediments at ambient and cryogenic temperatures, Physica B Condens. Matter 208 (1995) 309–310.
[55] M.-P. Isaure, A. Laboudigue, A. Manceau, G. Sarret, C. Tiffreau, P. Trocellier, G. Lamble, J.-L. Hazemann, D. Chateigner, Quantitative Zn speciation in a contaminated dredged sediment by μ-PIXE, μ-SXRF, EXAFS spectroscopy and principal component analysis, Geochim. Cosmochim. Acta 66 (2002) 1549–1567.
[56] D.A. Dzombak, F.M. Morel, Surface Complexation Modeling: Hydrous Ferric Oxide, John Wiley & Sons, 1990.
[57] J.A. Davis, J.A. Coston, D.B. Kent, C.C. Fuller, Application of the surface complexation concept to complex mineral assemblages, Environ. Sci. Technol. 32 (1998) 2820–2828.
[58] J.A. Davis, D. Kent, Surface complexation modeling in aqueous geochemistry, Rev. Mineral. Geochem. 23 (1990) 177–260.
[59] D. Span, J.F. Gaillard, An investigation of a procedure for determining carbonate bound trace metals, Chem. Geol. 56 (1986) 135–141.
[60] T.A. Al, C.J. Martin, D.W. Blowes, Carbonate-mineral/water interactions in sulfide-rich mine tailings, Geochimica Et Cosmochimica Acta 64 (2000) 3933–3948.
[61] E. Peltier, A.L. Dahl, J.-F. Gaillard, Metal speciation in anoxic sediments: when sulfides can be construed as oxides, Environ. Sci. Technol. 39 (2005) 311–316.
[62] S.L. Simpson, J. Rosner, J. Ellis, Competitive displacement reactions of cadmium, copper, and zinc added to a polluted, sulfidic estuarine sediment, Environ. Toxicol. Chem. 19 (2000) 1992–1999.
[63] O.J. Hao, J.M. Chen, L. Huang, R.L. Buglass, Sulfate-reducing bacteria, Crit. Rev. Environ. Sci. Technol. 26 (1996) 155–187.
[64] L.G. Sillen, A.E. Martell, J. Bjerrum, Stability constants of metal-ion complexes, Chemical Society, (1964).
[65] L. Toran, R.F. Harris, Interpretation of sulfur and oxygen isotopes in biological and abiological sulfide oxidation, Geochim. Cosmochim. Acta 53 (1989) 2341–2348.
[66] W. Ghosh, B. Dam, Biochemistry and molecular biology of lithotrophic sulfur oxidation by taxonomically and ecologically diverse bacteria and archaea, FEMS Microbiol. Rev. 33 (2009) 999–1043.
[67] C. Heidel, M. Tichomirowa, C. Breitkopf, Sphalerite oxidation pathways detected by oxygen and sulfur isotope studies, Appl. Geochem. 26 (2011) 2247–2259.
[68] P.C. Rath, R.K. Paramguru, P.K. Jena, Kinetics of dissolution of zinc sulphide in aqueous ferric chloride solution, Hydrometallurgy 6 (1981) 219–225.
[69] M. Boon, M. Snijder, G.S. Hansford, J.J. Heijnen, The oxidation kinetics of zinc sulphide with Thiobacillus ferrooxidans, Hydrometallurgy 48 (1998) 171–186.
[70] T.A. Fowler, F.K. Crundwell, Leaching of Zinc Sulfide by Thiobacillus ferrooxidans: Experiments with a Controlled Redox Potential Indicate No Direct Bacterial Mechanism, Appl. Environ. Microbiol. 64 (1998) 3570–3575.
[71] O. Garcia Jr, J.M. Bigham, O.H. Tuovinen, Sphalerite oxidation by Thiobacillus fertooxidans and Thiobacillus thiooxidans, Can. J. Microbiol. 41 (1995) 578–584.
[72] P.C. Singer, W. Stumm, Acidic mine drainage: the rate-determining step, Science 167 (1970) 1121–1123.
[73] F.J. Millero, S. Sotolongo, M. Izaguirre, The oxidation kinetics of Fe(II) in seawater, Geochimica et Cosmochimica Acta 51 (1987) 793–801.
[74] N. Nakai, M.L. Jensen, The kinetic isotope effect in the bacterial reduction and oxidation of sulfur, Geochimica et Cosmochimica Acta 28 (1964) 1893–1912.
[75] Y. Konishi, Y. Takasaka, S. Asai, Kinetics of growth and elemental sulfur oxidation in batch culture of thiobacillus ferrooxidans, Biotechnol. Bioeng. 44 (1994) 667–673.
[76] Y. Konishi, S. Asai, N. Yoshida, Growth Kinetics of Thiobacillus thiooxidans on the Surface of Elemental Sulfur, Appl. Environ. Microbiol. 61 (1995) 3617–3622.
[77] R. Gourdon, N. Funtowicz, Kinetic model of elemental sulfur oxidation by Thiobacillus thiooxidans in batch slurry reactors, Bioprocess Eng. 18 (1998) 241–249.
[78] T. Kai, Y.-i. Suenaga, A. Migita, T. Takahashi, Kinetic model for simultaneous leaching of zinc sulfide and manganese dioxide in the presence of iron-oxidizing bacteria, Chem. Eng. Sci. 55 (2000) 3429–3436.
[79] E.D. Burton, R.T. Bush, L.A. Sullivan, R.K. Hocking, D.R. Mitchell, S.G. Johnston, R. Fitzpatrick, M. Raven, S. McClure, L. Jang, Iron-monosulfide oxidation in natural sediments: resolving microbially mediated S transformations using XANES, electron microscopy, and selective extractions, Environ. Sci. Technol. 43 (2009) 3128–3134.
[80] S.A. Carroll, P.A. O'day, M. Piechowski, Rock-water interactions controlling zinc, cadmium, and lead concentrations in surface waters and sediments, US Tri-State Mining District. 2. Geochemical interpretation, Environ. Sci. Technol. 32 (1998) 956–965.
[81] E.D. Burton, R.T. Bush, L.A. Sullivan, Acid-volatile sulfide oxidation in coastal flood plain drains: iron-sulfur cycling and effects on water quality, Environ. Sci. Technol. 40 (2006) 1217–1222.
[82] K.S. Smith, Metal sorption on mineral surfaces: an overview with examples relating to mineral deposits, The Environmental Geochemistry of Mineral Deposits. Part B: Case Studies and Research Topics 6 (1999), pp. 161–182.
[83] Q.-G. Tan, C. Ke, W.-X. Wang, Rapid assessments of metal bioavailability in marine sediments using coelomic fluid of sipunculan worms, Environ. Sci. Technol. 47 (2013) 7499–7505.
[84] F. Tack, M.G. Verloo, Chemical speciation and fractionation in soil and sediment heavy metal analysis: a review, Int. J. Environ. Anal. Chem. 59 (1995) 225–238.

Effects of Resuspension on the Mobility and Chemical Speciation of Zn in Contaminated Sediments

Supporting Information

Minwei Xie[1,2,*], Marco A. Alsina[1,3], Jeffrey Yuen[1,4], Aaron I. Packman[1], Jean-Francçois Gaillard[1,*]

[1]Department of Civil and Environmental Engineering, Northwestern University, 2145 Sheridan Road, Evanston, IL 60208-3109, USA

[2]Marine Environmental Laboratory, Shenzhen Research Institute, The Hong Kong University of Science and Technology, Shenzhen 518000, China

[3]Department of Construction Engineering and Management, Faculty of Engineering, University of Talca, Curicó, Chile

[4]Present Address: Arcadis, 200 South Michigan Ave, Suite 2000, 60604 Chicago IL, USA

* Corresponding authors:

Minwei Xie, minwei.xie@qq.com

Jean-François Gaillard, jf-gaillard@northwestern.edu

This supporting information consists of 26 pages, including 7 figures and 7 tables:

Table S1. Sampling scheme of the resuspension experiment. Sediments for AVS determination (marked with #) were sampled from separate bottles but conducted simultaneously. Other parameters marked with * were determined in samples from common sources.

Time (h)	DO	pH	Dissolved metals	SO_4^{2-}	Total Metal	AVS	Zn and Fe speciation
1	*	*	*	*	*		*
2	*	*	*	*	*		
3	*	*	*	*	*		
4	*	*	*	*	*		
5	*	*	*	*	*		*
13	*	*	*	*	*	#	
25	*	*	*	*	*		*
37	*	*	*	*	*	#	
49	*	*	*	*	*		*
61	*	*	*	*	*	#	
73	*	*	*	*	*		
85	*	*	*	*	*	#	*
97	*	*	*	*	*		
109.5	*	*	*	*	*	#	
121	*	*	*	*	*		*
135	*	*	*	*	*	#	
145.5	*	*	*	*	*		*
326	*	*	*	*	*	#	*

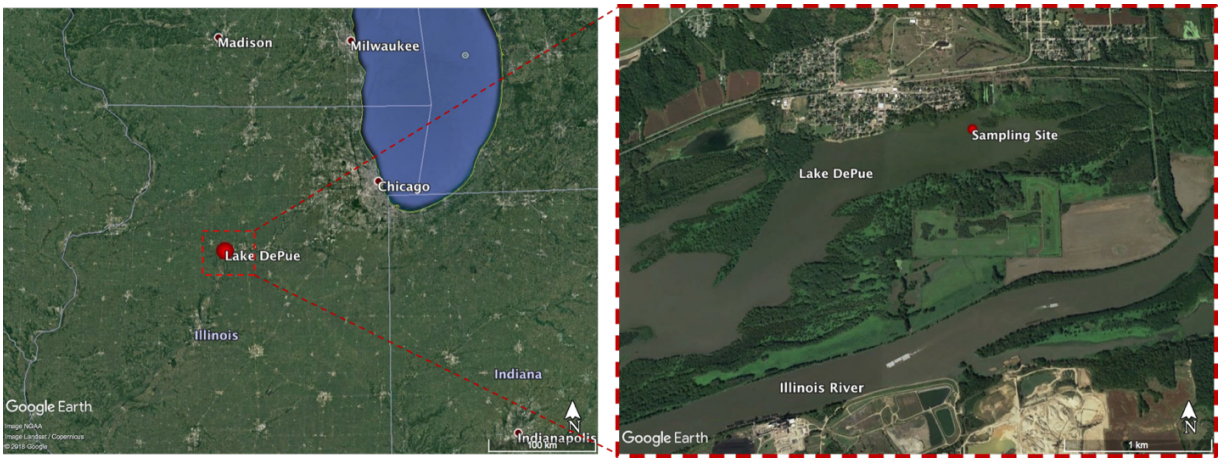

Figure S1. Aerial photography of Lake DePue and the sampling site (41°19'8.04"N, 89°18'39.35"W) (Google Earth, Retrieved on September 10, 2018).

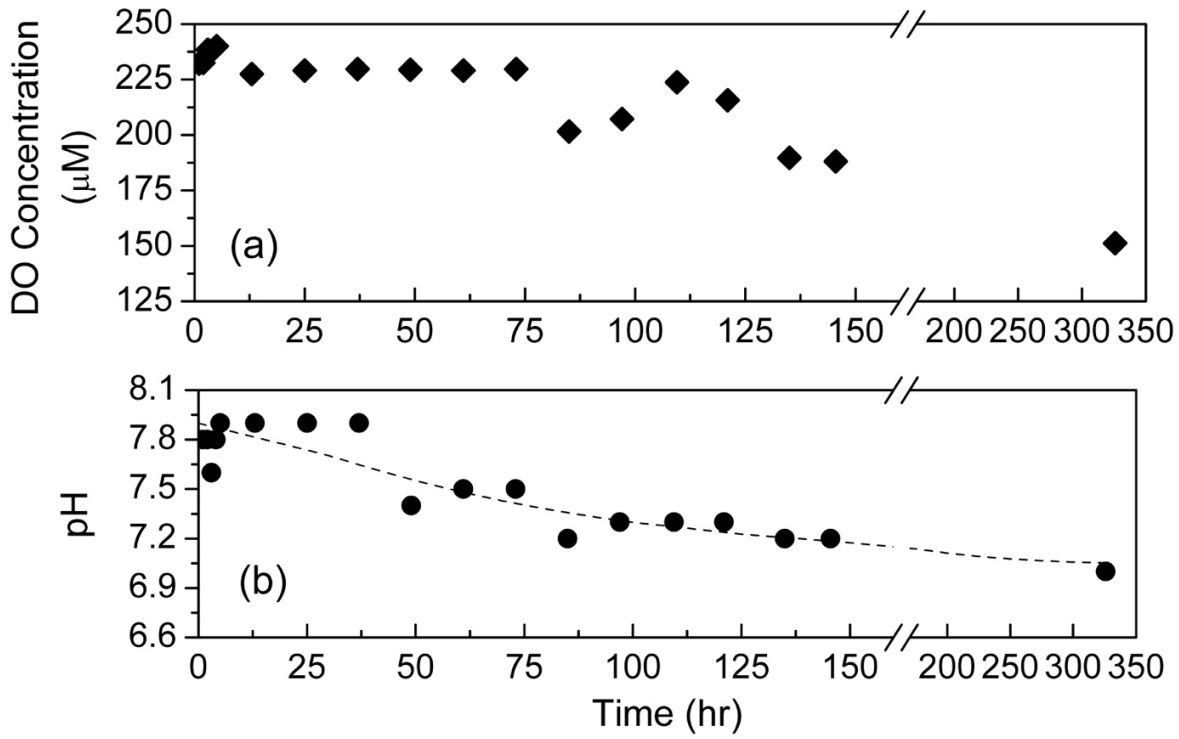

Figure S2. Evolution of dissolved oxygen (DO) concentration (a) and pH (b) during the resuspension experiment. Dashed line in (b) represents the resulting pH from the geochemical model.

Principal component analysis (PCA) and target transformation (TT) analysis of sample Zn K edge EXAFS spectra.

PCA analysis was performed on the entire dataset of sample EXAFS spectra (3 to 10 $Å^{-1}$). The output parameters for the first nine abstract components (C1-C9), including eigenvalues, the variance, the Malinowski indicator value (IND),[1] are shown in Table S2. Eigenvalues of the abstract components decreased from C1 to C9, indicating declining importance of the abstract component in reproducing the dataset. The parameter IND decreased and then increased, and reached minimum at C3, indicating the first three principal components (C1-C3) are necessary to reconstruct the sediment sample spectra.[1, 2] Components C1-C3 together accounted for 99.43% of the sample spectra signal and inclusion of other components (C4-C9) only marginally increased the fractions of variance. Therefore, C1-C3 were selected for TT analysis of the reference spectra.

TT analysis with the abstract components (C1-C3) were performed on 9 reference spectra to identify reference standards for linear combination fitting (LCF) (Figure S4). Targeting results were primarily evaluated with the R values, also known as normalized sum-squared residual (NSS) values, and also assessed by visual comparison between the target spectra and reference spectra. Among the 9 reference spectra, ZnS, $Zn_5(CO_3)_2(OH)_6$ and Zn-Goethite had the smallest R values. Considering Zn-Goethite and Zn-HFO showed very similar EXAFS structure, and freshly formed ferrihydrite had higher affinity for metals than crystalline goethite, we selected Zn-HFO instead of Zn-Goethite for the linear combination fit. This was further supported by the evidence that ferrihydrite, rather than goethite, was identified as a component Fe species in the sediments (*cf.* Figure S5). Although PCA analysis indicated that only three principle components were necessary to reconstruct the sample spectra, our previous work studying Zn speciation in Lake DePue sediments also identified Zn-aq as a major component species. Therefore, ZnS – Zn-S,

$Zn_5(CO_3)_2(OH)_6$ – Zn-CO_3, Zn-HFO, and Zn-aq were used as reference spectra to decompose the sample spectra.

Least-squares LCF with the reference spectra — Zn-S, Zn-CO_3, Zn-HFO, and Zn-aq — were performed on EXAFS spectra (3 to 10 $Å^{-1}$). The EXAFS spectra and fitted curve of sediment samples are displayed in Figure 3. Proportions of each Zn species are shown in Figure 4a and Table S3. Residuals of the fits were assessed by means of the R values, as shown in Table S3. As indicated by the R values, which are all smaller than 0.05, the reconstructed curves fit the original EXAFS spectra very well.

Table S2. Principal component analysis results for sample Zn K edge EXAFS spectra.

Component #	Eigenvalue	% of Variance	IND ($\times 10^{-4}$)
C1	8.280773	92.01	3.945
C2	0.581465	98.47	2.411
C3	0.086715	99.43	2.158
C4	0.022572	99.68	2.542
C5	0.012009	99.82	3.377
C6	0.00652	99.89	5.387
C7	0.004609	99.94	10.87
C8	0.003026	99.97	4.047
C9	0.002309	100	–

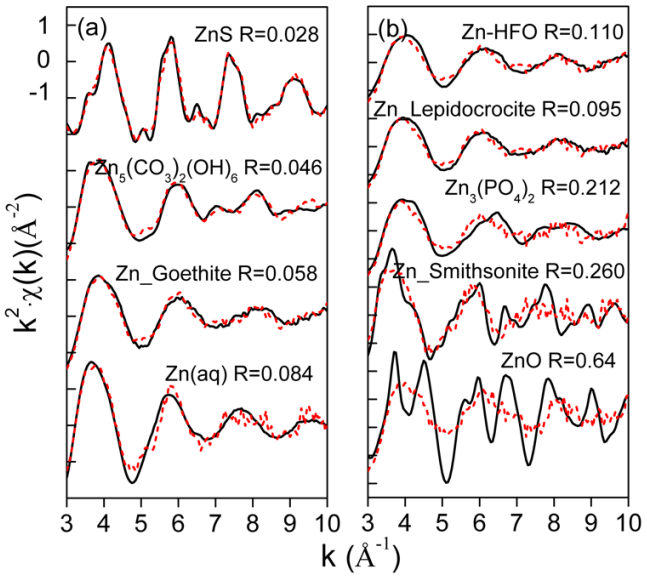

Figure S3. Zn K-edge EXAFS spectra (full lines), target transformations (dashed lines), and R values of 9 reference compounds. $\mathbf{R = \sum_i [k^2 \chi(k_i)_{data} - k^2 \chi(k_i)_{fit}]^2 / \sum_i [k^2 \chi(k_i)_{data}]^2}$.

Table S3. Zn speciation determined by LCF with EXAFS spectra

Resuspension time (hr)	Zn-S (%)	Zn-CO_3 (%)	Zn-aq (%)	Zn-HFO (%)	R ($\times 10^{-2}$)
0	68.6±1.8	21.6±3.8	9.7±2.9	0	3.91
1	56.9±1.7	31.7±6.7	4.4±2.7	6.9±6.2	3.52
5	56.0±1.4	26.2±6.0	7.9±2.4	9.9±5.7	2.89
25	49.2±1.5	30.9±6.1	4.3±2.5	15.6±5.7	3.18
49	35.9±1.4	23.2±6.0	8.2±2.4	32.8±5.6	3.36
85	23.3±1.3	47.7±5.3	8.9±2.1	20.1±4.9	2.76
121	11.1±1.5	40.5±5.9	7.7±2.3	40.7±5.5	3.58
145.5	13.6±1.4	47.2±5.8	26.0±2.3	13.2±5.4	2.98
326	8.3±1.9	59.9±3.9	31.9±3.0	0	4.92

Principal component analysis (PCA) and target transformation (TT) analysis of sample Fe K edge derivative XANES spectra

PCA analysis was also performed on the entire dataset of sample Fe K edge derivative XANES spectra (-20 to 30 eV above absorption edge). The output parameters for the first nine abstract components (C1-C9), including eigenvalues, the variance, the Malinowski indicator value (IND),[1] are shown in Table S4. The parameter IND decreased and then increased, and reached minimum at C2, indicating the first two principal components (C1-C2) are necessary to reconstruct the sediment sample spectra. Components C1-C2 together accounted for 99.87% of the sample spectra signal while the other components (C3-C9) together only accounted for 0.13% of the variance. Therefore, C1-C2 were selected for TT analysis of the reference spectra.

TT analysis with the abstract components (C1-C2) were performed on 9 reference spectra to identify reference standards for linear combination fitting (LCF) (Figure S5). Targeting results were primarily evaluated with the R values, and also assessed by visual comparison between the target spectra and reference spectra. Among the 9 reference spectra, aegirine ($NaFeSi_2O_6$) and ferrihydrite had the smallest R values and they show distinct spectroscopic structures in the derivative XANES spectra. Aegirine is characterized by three oscillations near the absorption edge while ferrihydrite has two peaks. Therefore, both aegirine and ferrihydrite were selected as references to decompose the sample spectra. While performing linear combination fitting (LCF) for the sample derivative XANES spectra, an additional species was added to the LCF if the resulting R value decreased by at least 10%.[2] Here, we also observed that inclusion of vivianite ($Fe_3(PO_4)_2 \cdot 8H_2O$) in the first sediment sample spectrum (t = 0 h) decreased R value from 0.0274 to 0.0206 (24.8% decrease). Therefore, vivianite was also selected as a reference for the LCF

reconstruction of the first sample spectrum. Inclusion of vivianite in LCF reconstruction of other sample spectra did not improve the fit quality and thus was not used.

Least-squares LCF with the reference spectra — aegirine, ferrihydrite, and vivianite — were performed on derivative XANES spectra (-20 to 30 eV above the absorption edge). The derivative XANES spectra and fitted curve of sediment samples are displayed in Figure 2a. Proportions of each Zn species are shown in Figure 2b and Table S5. Residuals of the fits were assessed by means of the R values, as shown in Table S5. As indicated by the R values, which are all smaller than 0.05, the reconstructed curves fit the original derivative XANES spectra very well.

Table S4. Principal component analysis results for sample Fe K edge derivative XANES spectra.

Component #	Eigenvalue	% of Variance	IND ($\times 10^{-4}$)
C1	8.952035	99.47	1.02
C2	0.036037	99.87	0.71
C3	0.004740	99.92	0.81
C4	0.003651	99.96	0.90
C5	0.001187	99.97	1.28
C6	0.000890	99.98	2.07
C7	0.000594	99.99	4.39
C8	0.000502	100	16.11
C9	0.000366	100	–

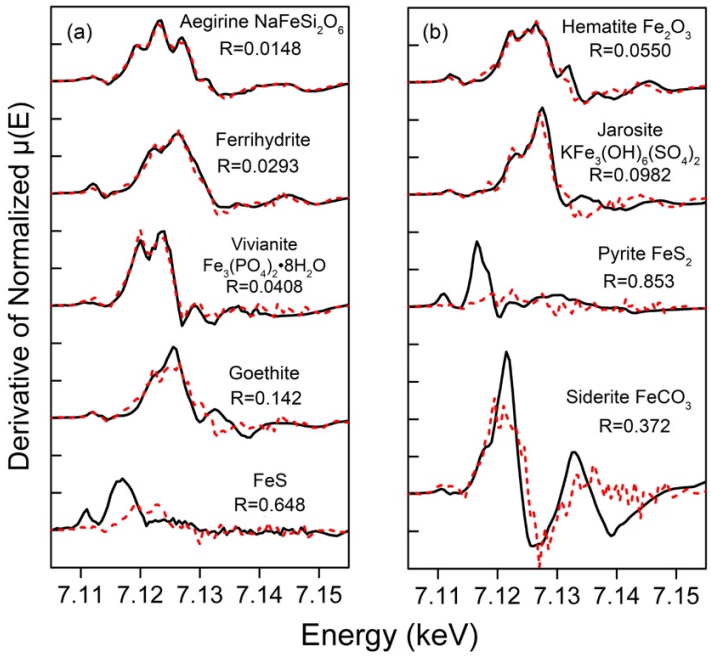

Figure S4. Fe K-edge derivative XANES spectra (full lines), target transformations (dashed lines), and R values of 9 reference compounds. $\mathbf{R} = \sum_i[\boldsymbol{Observed} - \boldsymbol{Fit}]^2 / \sum_i[\boldsymbol{Observed}]^2$.

Table S5. Fe speciation determined by LCF with derivative XANES spectra.

Resuspension time (hr)	Aegirine (%)	Ferrihydrite (%)	Vivianite (%)	R ($\times 10^{-2}$)
0	67.2±4.7	18.0±3.4	14.7±5.8	2.06
1	65.5±2.6	34.5±3.9	0	1.50
5	69.3±2.1	30.7±3.1	0	1.05
25	70.3±2.5	29.7±3.8	0	1.41
49	70.9±2.1	29.1±3.5	0	1.06
85	56.5±2.6	43.5±3.9	0	1.53
121	52.9±2.9	47.1±4.1	0	1.82
145.5	65.2±2.3	34.8±3.7	0	1.26
326	63.5±2.7	36.5±3.9	0	1.58

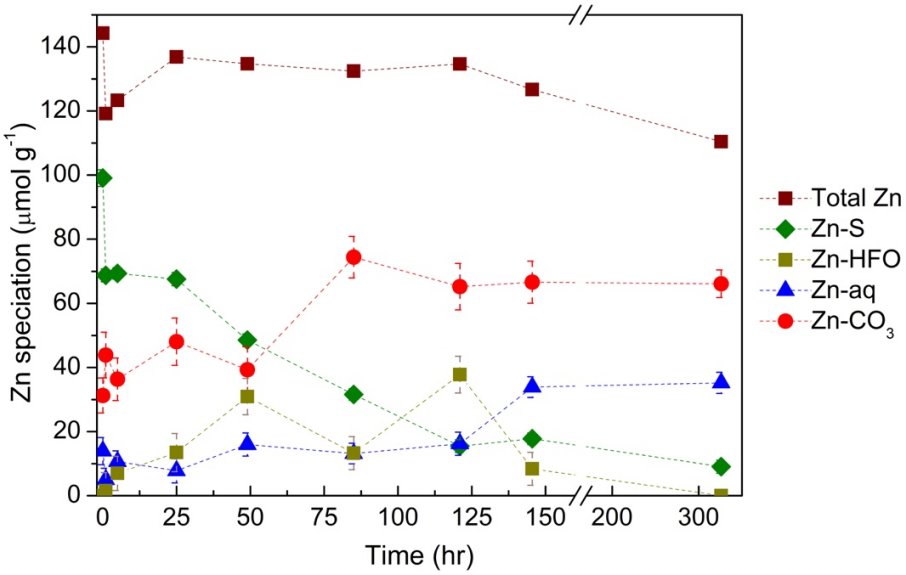

Figure S5. Estimated concentration of Zn species in the suspended sediments during the resuspension experiment.

AVS oxidation

Oxidation of anoxic sediments during sediment resuspension led to decrease in acid volatile sulfide (AVS) concentrations (Figure S6). The initial AVS concentration of 91 μmol/g decreased to 50 μmol/g after 15 h. The rate of AVS loss then decreased and AVS dropped to 5 μmol/g over the remained of the experimental duration. Overall, temporal evolution of AVS matched the Zn-S concentration profiles calculated from Zn speciation data (Figure S6), also suggesting that ZnS was the predominant species of AVS in sediments.

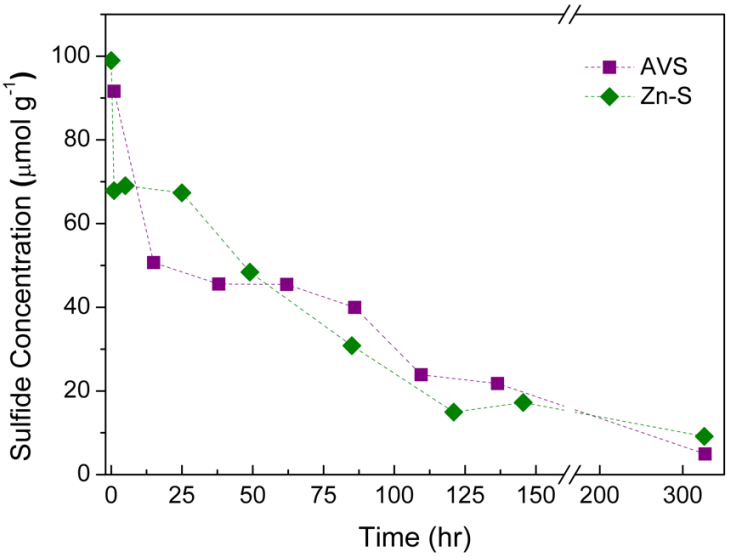

Figure S6. AVS oxidation and Zn-S concentration.

Implementation details of the kinetic geochemical model

Figure S7 presents the schematics for the non-linear least-squares fitting procedure used to derive the parameters of the kinetic geochemical model, namely (i) the linear rate constant (*K*) for the oxidation of $ZnS_{(s)}$, (ii) The concentration of hydrozincite ($Zn_5(OH)_6(CO_3)_{2(s)}$) and Zn bound to natural organic matter in the mineral assemblage, and (iii) the residual non-reactive concentrations of $[\equiv HFO]$ and hydrozincite. The figure of merit used to assess the quality of the fits is the reduced-χ^2,

$$red\text{-}\chi^2 = \frac{1}{(n-d)} \sum_{i=1}^{n} \frac{(obs_{y_i} - mod_{y_i})^2}{w_i}$$

Where *n* corresponds to the total number of observed values, *d* corresponds to the number of variables for the model, obs_y and mod_y correspond to the observed and modeled values, respectively, and w_i corresponds to the weight factor of each value. The fitting procedure can be divided in 3 stages, described as follows.

Stage 1: Estimation of the linear kinetic rate K.

The initial composition of the water in the geochemical model was derived from the water quality data of LDP water, presented in Table 1. Since the concentration of dissolved sulfate does not depend significantly from pH and presence of reactive surfaces, the estimation of the linear rate (*K)* was performed directly via a least-squares fitting step. Equation 1 provides the coupling between the oxidation of $ZnS_{(s)}$ and the consequential release of dissolved sulfate, which was then fitted considering the evolution of dissolved sulfate (mM) during the resuspension experiment as the observed values.

Stage 2: Estimation of mineral assemblage concentrations.

Once the linear rate was estimated, the concentration of hydrozincite and Zn bound to organic matter in the mineral assemblage was estimated considering the evolution of both dissolved Zn (μM) and pH (a.u.) during the resuspension experiment as the observed values. Adsorption of Zn^{2+} on ferrihydrite was modeled using surface-complexation approach, considering a concentration of 610 μmol/g sediment. This value was chosen based on the total recoverable iron concentration measured in the sediments (610±27 μmol/g) (Table 1), which represents the iron concentration recovered with concentrated HNO_3 solution following USEPA method 3051A. The aegirine mineral, also known as sodium iron silicate, cannot be recovered with this method, and therefore, the total recoverable iron concentration measured in Lake DePue sediments may represent the concentration of HFO. This surface-complexation approach requires knowledge of the binding constants between adsorbate and adsorbent, and other intrinsic properties of adsorbent surface such as capacitances, specific surface area, and surface site densities.[3] As recommended by Dzombak and Morel[4], the following parameters were used in the model: specific surface = 10,000 m^2/mol Fe, high-affinity site density = 0.005 mol sites/mol Fe, low-affinity site density = 0.2 mol sites/mol Fe. An additional organic phase was considered for adsorption of Zn^{2+} at the onset of the experiment. For this case the adsorption was modeled considering a complexation reaction in which the amount of ligand was fitted. The equilibrium constant considered for the complexation reaction is presented in Table S6.

A weighted least-squares fitting was employed to compensate for the different units of the observed values. Weight factors of 0.1 and 1.0 were considered for the pH and dissolved Zn, respectively, on the objective function.

Stage 3: Estimation of residual concentrations.

Finally, the results from the Zn K-edge EXAFS analysis of the resuspended sediments were considered to determine the non-reactive residual concentrations of ferrihydrite and hydrozincite. Note that this procedure is not coupled with the geochemical model, since it estimates residual fractions that are non-reactive.

The following table summarizes the principal reactions considered for the surface complexation model. The equilibrium constants for HFO were obtained from Dzombak and Morel[4], while the equilibrium constant for the organic phase (OM) was adapted from the humic ion-binding model developed by Tipping et al.[5]

Finally, Table S7 summarizes the results of the geochemical model in terms of the fitted parameters and residuals per each step.

Table S6. Principal surface complexation reactions considered in the geochemical model.

Reaction	Log K
Ferrihydrite (HFO)[a]	
$[\equiv HFO\_w]OH + H^+ \leftrightarrow [\equiv HFO\_w]\ OH_2^+$	7.29
$[\equiv HFO\_w]OH \leftrightarrow [\equiv HFO\_w]O^- + H^+$	-8.93
$[\equiv HFO\_s]OH + H^+ \leftrightarrow [\equiv HFO\_s]\ OH_2^+$	7.29
$[\equiv HFO\_s]OH \leftrightarrow [\equiv HFO\_s]O^- + H^+$	-8.93
$[\equiv HFO\_w]OH + Zn^{2+} \leftrightarrow [\equiv HFO\_w]OZn^{+-} + H^+$	-1.99
$[\equiv HFO\_s]OH + Zn^{2+} \leftrightarrow [\equiv HFO\_s]OZn^{+-} + H^+$	0.99
Organic phase (OM)	
$OM^- + Zn^{2+} \leftrightarrow OMZn^+$	6.00

[a] HFO considers a weak (w) and a strong (s) adsorption site

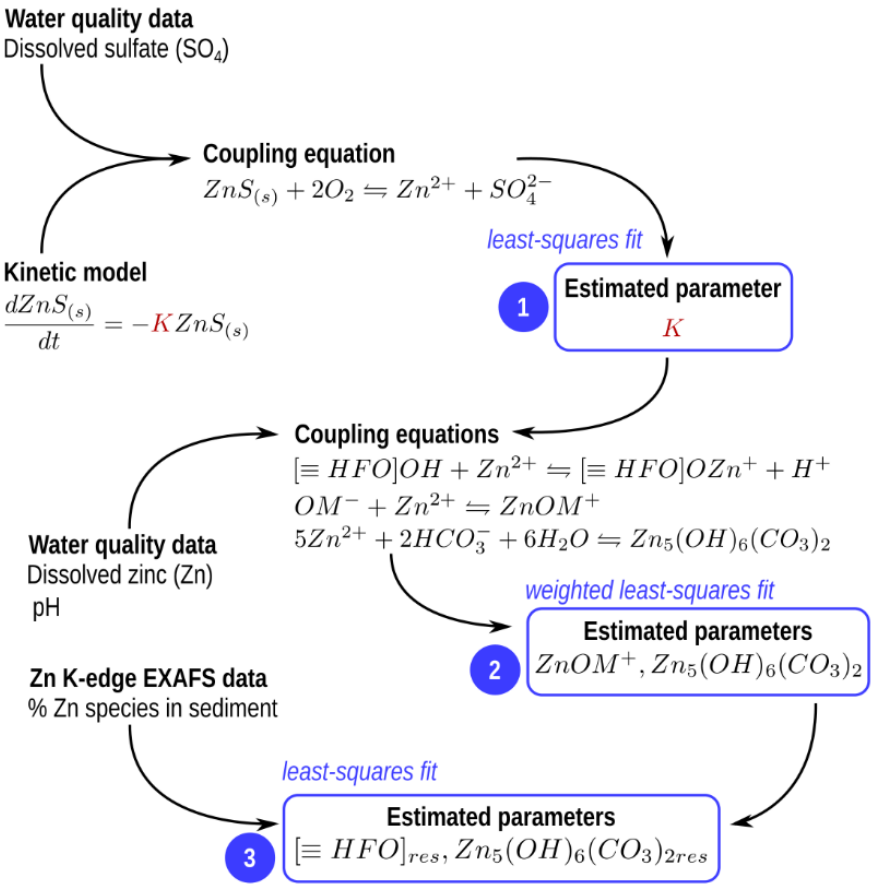

Figure S7. Schematics of the non-linear least squares fitting procedure for the kinetic geochemical model. Blue boxes indicate the least-squares steps.

Table S7. Parameters and residuals obtained by the geochemical model.

Stage	Parameter	Unit	Value	*red-*χ^2
1	K	hr^{-1}	$3.01 \pm 0.12 \times 10^{-7}$	0.010
2	OM^-	mol lt^{-1}	$0.28 \pm 0.04 \times 10^{-3}$	24.146
3	$[\equiv HFO]_{res}$	moles	$0.73 \pm 0.08 \times 10^{-4}$	0.009
	$Zn_5(OH)_6(CO_3)_{2res}$	moles	$0.08 \pm 0.07 \times 10^{-4}$	

Changes of pH

As seen in Figure S3, the oxidation of sediment resulted in a reduction of pH from 7.8 to ~7.0. pH decrease is attributed in the geochemical model to acidification caused by two processes: (i) Zn complexation with bicarbonate species, and (ii) Zn adsorption onto HFO,

$$Zn^{2+} + HCO_3^- \leftrightarrow ZnCO_{3(aq)} + H^+ \quad (S1)$$

$$Zn^{2+} + 2HCO_3^- \leftrightarrow Zn(CO_3)_2^{2-} + 2H^+ \quad (S2)$$

$$\left[\equiv HFO\right]OH + Zn^{2+} \leftrightarrow \left[\equiv HFO\right]OZn^+ + H^+ \quad (S3)$$

Although oxidative precipitation of Fe(II) to $Fe(OH)_3$ has been recognized as an important process that releases acidity in other studies,[3, 6-8] it was not accounted in the current geochemical model with the assumption of pre-existing Fe(III) minerals in the sediment. This assumption is justified by the evidence that the valence state of Fe species in the sediments was predominantly +3 over the course of resuspension experiment (for t =1 to 326 h) (Figure 2 c). The presence of Fe(II) as vivianite in the bulk sediment was rapidly eliminated within 1 h after the onset of resuspension experiments. Although oxidation of Fe(II) during this 1 h period released acidity to the water, we did not observe any drastic decrease in pH (Figure S3b). Several mechanisms might be postulated: i) Phosphate was associated with Fe(II) in the vivianite minerals. As vivianite was converted to ferrihydrite, PO_4^{3-} may be converted to HPO_4^{2-}/ $H_2PO_4^-$ and function as a buffer to the system; ii) LDP water has high alkalinity, which also buffered the solution pH; (iii) Carbonate minerals in sediments, such as calcite, dolomite, may also consume the acidity released during the Fe(II) oxidation.

References

1. Malinowski, E. R., Determination of the number of factors and the experimental error in a data matrix. *Analytical Chemistry* **1977,** *49*, (4), 612-617.

2. Van Damme, A.; Degryse, F.; Smolders, E.; Sarret, G.; Dewit, J.; Swennen, R.; Manceau, A., Zinc speciation in mining and smelter contaminated overbank sediments by EXAFS spectroscopy. *Geochimica et cosmochimica acta* **2010,** *74*, (13), 3707-3720.

3. Smith, K. S., Metal sorption on mineral surfaces: an overview with examples relating to mineral deposits. *The Environmental Geochemistry of Mineral Deposits. Part B: Case Studies and Research Topics* **1999,** *6*, 161-182.

4. Dzombak, D. A.; Morel, F. M., *Surface complexation modeling: hydrous ferric oxide*. John Wiley & Sons: 1990.

5. Tipping, E.; Lofts, S.; Sonke, J., Humic Ion-Binding Model VII: a revised parameterisation of cation-binding by humic substances. *Environmental Chemistry* **2011,** *8*, (3), 225-235.

6. Burton, E. D.; Bush, R. T.; Sullivan, L. A.; Hocking, R. K.; Mitchell, D. R.; Johnston, S. G.; Fitzpatrick, R.; Raven, M.; McClure, S.; Jang, L., Iron-monosulfide oxidation in natural sediments: resolving microbially mediated S transformations using XANES, electron microscopy, and selective extractions. *Environmental science & technology* **2009,** *43*, (9), 3128-3134.

7. Carroll, S. A.; O'day, P. A.; Piechowski, M., Rock-water interactions controlling zinc, cadmium, and lead concentrations in surface waters and sediments, US Tri-State Mining District. 2. Geochemical interpretation. *Environmental science & technology* **1998,** *32*, (7), 956-965.

8. Burton, E. D.; Bush, R. T.; Sullivan, L. A., Acid-volatile sulfide oxidation in coastal flood plain drains: iron-sulfur cycling and effects on water quality. *Environmental Science & Technology* **2006,** *40*, (4), 1217-1222.